International Journal of Nanomedicine

Dovepress
open access to scientific and medical research

Open Access Full Text Article

ORIGINAL RESEARCH

TEM Studies on Antibacterial Mechanisms of Black Phosphorous Nanosheets

This article was published in the following Dove Press journal:
International Journal of Nanomedicine

Abhijit H Phakatkar[1]
Emre Firlar[1–3]
Laura Alzate[1,†]
Boao Song[2]
Surya Narayanan[1]
Ramin Rojaee[2]
Tara Foroozan[2]
Ramasubramonian Deivanayagam[2]
David James Banner[1]
Reza Shahbazian-Yassar[2]
Tolou Shokuhfar[1]

[1]Department of Bioengineering, University of Illinois at Chicago, Chicago, IL 60607, USA; [2]Department of Mechanical and Industrial Engineering, University of Illinois at Chicago, Chicago, IL 60607, USA; [3]Institute for Quantitative Biomedicine, Rutgers University, Piscataway, NJ 08854, USA

[†]Laura Alzate passed away on October 20, 2019

Purpose: Recently, two-dimensional (2D) nanomaterials are gaining tremendous attention as novel antibacterial platforms to combat against continuously evolving antimicrobial resistance levels. Among the family of 2D nanomaterials, black phosphorus (BP) nanosheets have demonstrated promising potential for biomedical applications. However, there is a need to gain nanoscale insights of the antibacterial activity of BP nanosheets which lies at the center of technical challenges.

Methods: Ultra-large BP nanosheets were synthesized by liquid-exfoliation method in the eco-friendly deoxygenated water. Synthesized BP nanosheets were characterized by TEM, AFM, and Raman spectroscopy techniques and their chemical stability was evaluated by EDS and EELS elemental analysis. The antibacterial activity of BP nanosheets was evaluated at nanoscale by the ultramicrotome TEM technique. Further, HAADF-STEM image and EDS elemental line map of the damaged bacterium were utilized to analyze the presence of diagnostic ions. Supportive SEM and ATR-FTIR studies were carried out to confirm the bacterial cell wall damage. In vitro colony counting method was utilized to evaluate the antibacterial performance of ultra-large BP nanosheets.

Results: Elemental EELS and EDS analysis of BP nanosheets stored in deoxygenated water confirmed the absence of oxygen peak. TEM studies indicate the various events of bacterial cell damage with the lost cellular metabolism and structural integrity. Colony counting test results show that as-synthesized BP nanosheets (100 μg/mL) can kill ~95% bacteria within 12 hours.

Conclusion: TEM studies demonstrate the various events of *E. coli* membrane damage and the loss of structural integrity. These events include the BP nanosheets interaction with the bacterial cell wall, cytoplasmic leakage, detachment of cytoplasm from the cell membrane, reduced density of lipid bilayer and agglomerated DNA structure. The EDS elemental line mapping of the damaged bacterium confirms the disrupted cell membrane permeability and the lost cellular metabolism. SEM micrographs and ATR-FTIR supportive results confirm the bacterial cell wall damage.

Keywords: phosphorene, transmission electron microscopy, black phosphorus nanosheet, two-dimensional materials, antibacterial

Correspondence: Tolou Shokuhfar
Department of Bioengineering, University of Illinois at Chicago, Chicago, IL 60607, USA
Tel +1 312 413 9872
Email tolou@uic.edu

Reza Shahbazian-Yassar
Department of Mechanical and Industrial Engineering, University of Illinois at Chicago, IL 60607, USA
Tel +1 312 996 3440
Email rsyassar@uic.edu

Introduction

The evolving antimicrobial resistance levels for pathogenic bacteria have been a compelling global challenge.[1,2] Over the period, the scientists have studied the intrinsic and adaptive drug-resistance abilities of bacteria mainly related with modification in the bacterial cell structure, mutation to prevent drug and antibiotics targets, and direct alteration or inactivation of drug molecules.[3,4] Biochemical mechanisms of bacterial antibiotic resistance can be categorized as enzymatic inactivation of antibiotic drug molecule, drug efflux pumps made-up with chromosome and/or plasmid, altering the intracellular target of drug by involving

ribosomes, metabolic enzymes, proteins for cell wall synthesis and DNA replication and chromosomal transfer by acquiring DNA from adjacent bacteria.[5] To counteract these mutating abilities of bacteria, in the past two decades, the research has been more focused on evaluating the antibacterial activities of various advanced nanomaterials against Gram-positive and Gram-negative bacteria by considering their advantages with material properties, surface charge and characteristics, shape, size, aspect ratio, dispersion abilities and reactivity with surrounding environmental conditions.[6,7,8]

Among various advanced nanomaterials, two-dimensional (2D) nanomaterials are considered to be promising and emerging anti-bacterial platforms, attributed with their benefits over high surface to volume ratio, plenty of surface-active sites and controlled toxicity.[9,10] In the family of 2D nanomaterials, the antibacterial activities of reduced graphene oxide (rGO) and graphene oxide (GO) nanocomposites are widely studied for their physical damage abilities against bacterial cell membranes and their capacity to produce reactive oxygen species (ROS), ascribed to the presence of surface functional groups and the large effective surface area.[11,12] Antibacterial activities of vertically aligned molybdenum disulfide (MoS_2) and manganese dioxide (MnO_2) 2D nanosheets show possible antibacterial mechanisms mainly associated with cell membrane oxidative damage with ROS and physical penetration into bacterial cell membrane.[9,10] Among the family of ROS, singlet oxygen ($^1O_2$), hydrogen peroxide (H_2O_2), hydroxyl radical ($OH\cdot$) and superoxide anion (O_2^-) are the strong oxidizing agents that can inhibit pathogens by damaging essential biomolecules and by triggering lipid peroxidation reactions.[13,14] The oxidative damage of cellular proteins and fatty acids caused by ROS is believed to be localized due to their respective instantaneous reactivities, limited diffusion and short lifetime periods.[14–16] Hence, it is unlikely for intracellular defensive enzymes to prevent the oxidative damage of cell membrane components located at a longer distance.[14] In the case of antioxidant enzymes within bacterial cells that eliminate $^1O_2$ have not evolved most likely due to its shorter lifetime as compared with remaining long-lived ROS species such as, O_2^-, peroxides and H_2O_2.[17] Lately, researchers have focused their attention towards the phosphorene, i.e. 2D exfoliated black phosphorus (BP) nanosheets associated with their unique attributes, such as ease of synthesis, high anisotropic charge carrier mobility, singlet oxygen generation capacity and nanosheets thickness-dependent tunable intrinsic bandgap which can be adjusted between zero bandgap graphene and wide bandgap transition metal dichalcogenides.[18–22] Few studies have evaluated the antibacterial activity of BP nanosheets.[18,22,23] Tan et al[22] have demonstrated the antibacterial activity of biofilm comprised BP nanosheets and poly(4-pyridonemethylstyrene) endoperoxide indicating controlled ROS release as the bacteria-killing mechanism in the controlled environment. Sun et al[18] have proved the excellent antibacterial activity of irradiated few-layer exfoliated BP nanosheets synthesized in the iso-propyl alcohol (IPA) media. The proposed mechanism involves shrinkage and damage to the bacterial cell membrane due to trapping or wrapping of microbes by BP nanosheets further suggesting facilitation of photothermal inactivation. Moreover, Xiong et al[23] have shown the scanning electron microscopy characterization of the time-dependent physical damage of bacterial cell membrane caused by exfoliated BP nanosheets, which were supported by membrane damage lactate dehydrogenase and intracellular ROS quantitative evaluations.

The available studies indicate that the cytotoxicity of exfoliated BP nanosheets needs to be investigated further. Some studies show that the cytotoxicity of BP nanosheets can be related mainly with the concentration of ROS generated upon contact with exfoliated BP nanosheets of thickness around 90 nm and lateral size of 800 nm.[24,25] Exfoliated BP nanosheets generate ROS in excessive amount upon UV irradiation. Produced ROS can build oxidative stress within fibroblast cells causing reduced enzyme activity, lipid peroxidation and DNA breakage.[25] On the other hand, in vivo and in vitro studies of BP nanosheets have demonstrated excellent cytocompatibility even at high concentrations with very negligible changes in the cellular morphology.[26–29] The degradation of oxidized BP nanosheets results in the production of either phosphoric acid (H_3PO_4) or phosphate derivatives, which are essential for maintaining physiological pH and cellular metabolism.[24,30,31] These advantages have motivated the studies for biomedical applications of BP nanosheets including drug delivery, biosensing, theranostics, bioimaging photothermal therapy applications.[32–37] By attributing to the biocompatibility, biodegradability and antimicrobial properties of BP nanosheets, we hypothesize their potential use as biocompatible filler constituents in the polymethyl methacrylate (PMMA) bone cement composite matrix to provide antimicrobial attributes, which can prevent postoperative bacterial infections and hence can help in reducing the burden of revision arthroplasty surgeries.

Herein, for the first time, we report the interaction of chemically stable few-layer BP nanosheets against the gram-negative *Escherichia coli* (*E. coli*) bacteria by transmission electron microscopy (TEM) technique. Our results provide nanoscale insights of structural damage caused by BP nanosheets to the bacterial cell membrane. TEM results also reveal the cytoplasmic leakage and deoxyribonucleic acid (DNA) agglomeration insightful observations. Complementary scanning electron microscopy (SEM) technique was utilized to confirm cell wall damage caused by BP nanosheets. The chemical analysis of damaged bacterial cell membrane was performed by using attenuated total reflectance-Fourier-transform infrared spectroscopy (ATR-FTIR) technique which has been briefly discussed in the supplementary information. The disrupted membrane permeability and the loss of cellular components are confirmed by analyzing the presence of diagnostic phosphorus, sulfur, chlorine and calcium ions evaluated with the energy-dispersive X-ray spectroscopy (EDS) elemental line mapping of the damaged bacterium in the high-angle annular dark-field (HAADF) – scanning transmission electron microscope (STEM) imaging mode. The study also indicates that by tuning the liquid exfoliation process parameters, it is possible to synthesize micron size few-layer BP nanosheets in the ecofriendly, non-toxic and biocompatible deoxygenated water media. Exfoliated BP nanosheets were characterized by Raman spectroscopy, TEM and atomic force microscopy (AFM) techniques in order to confirm their morphology. The chemical stability of as-synthesized BP nanosheets in the deoxygenated water was evaluated by using EDS and electron energy loss spectroscopy (EELS) techniques. In conclusion, our results show the structural and membrane damage caused by exfoliated few-layer BP nanosheets and the resultant events of the lost cellular metabolism which possibly played a crucial role in exhibiting the excellent antibacterial activity.

Materials and Methods

Materials

For obtaining deoxygenated water, Sigma-Aldrich, USA (W3500-1L) sterile-filtered water was utilized. Bulk BP crystals were purchased from smart elements (Art. Nr. 003058) from Vienna, Austria. For TEM EDS mapping and EELS characterizations, lacey carbon 300 mesh copper grids (LC300-CU-150) and lacey carbon 300 mesh gold grids (LC325-AU) were purchased from Electron Microscopy Sciences, USA. For Raman spectroscopy and AFM analysis, 500 μm thick silicon wafers (2379) were purchased from UniversityWafer, USA. For antibacterial tests, *Escherichia coli* (*E. coli*) K12 gram-negative bacteria strain (ATCC®29425™) was purchased from ATCC, USA. For preparing bacteria cultures, Luria Broth (Miller's LB Broth_L24040-500.0), molecular grade water (248700) and Luria Agar (Miller's LB Agar_L24020-500.0) were purchased from Research Products International (RPI), USA. For ultramicrotome resin-embedded sample preparation, EMBed-812 (Cat. #14120) embedding kit, glutaraldehyde 2.5% aqueous (Cat. # 16537–16), osmium tetroxide 2% aqueous solution (Cat. # 19152) and 200 mesh copper TEM grids (Cat. #EMS200-Cu) were purchased from Electron Microscopy Sciences, USA. For staining ultramicrotome resin samples, uranyl acetate 2% solution (Cat. # 22400–2) and lead citrate (Cat. # 17800) were procured from Electron Microscopy Sciences, USA. For bacteria SEM sample preparation, glutaraldehyde 2.5% in 0.1 M Phosphate buffer pH 7.4 (EMS catalog #16537-05) and hexamethyldisilazane reagent (EMS catalogue # 16700) were utilized.

Synthesis of Few-Layer BP Nanosheets in Deoxygenated Water

The synthesis of few-layer BP nanosheets was carried out in deoxygenated water by liquid exfoliation method in a similar manner as reported in earlier published work,[38,39] but by utilizing the altered process parameters in order to achieve large surface area ultrathin exfoliated BP nanosheets. Primarily, deoxygenated water was prepared by bubbling argon gas for 90 minutes in sterile-filtered water placed in a vacuum lined flask. The bulk BP crystals were grinded to powder with mortar-pestle in an argon-filled glovebox. The grinded BP powder was transferred to a container containing deoxygenated water by maintaining 1mg/mL concentration. The liquid exfoliation is carried out by using Fisher Scientific Sonic Dismembrator (Model 705) for 6 hours and by tuning operating parameters as 100W power at 20 kHz frequency and pulse mode operating time of 1s with 2s of time interval. The deoxygenated water temperature was maintained at 20°C during the exfoliation process. As-prepared exfoliated few-layer BP nanosheet samples were centrifuged at 800 rpm for 5 minutes and aliquoted in air-tight containers for further studies. During synthesis, the minimum exposure with atmospheric oxygen and light was maintained. The basis of synthesizing BP nanosheets by liquid exfoliation method in deoxygenated water is represented in Figure 1.

Material Characterization of Synthesized BP Nanosheets

Low-Magnification Transmission Electron Microscopy Analysis

The lateral dimensions and morphology of as-synthesized exfoliated BP nanosheets were evaluated by using the JEOL JEM 1220 transmission electron microscope (TEM). The samples were prepared by simply drop-casting 2 μL exfoliated few-layer BP suspension on lacey carbon (LC300-CU-150) grids and allowed to dry at room temperature. For TEM imaging, the incident beam energy of 80 keV was used to avoid possible damage caused by the electron beam.

Raman Spectroscopy Analysis

To characterize the exfoliated few-layer BP nanosheets, Raman spectroscopy was performed using Renishaw inVia Reflex micro-Raman spectrometer. The samples were prepared by using silicon wafer as a substrate. The diode-pumped solid-state laser with 532 nm excitation wavelength operated at 1.0 mW was focused on bulk BP crystal and exfoliated BP nanosheets by using a 50× objective lens.

Atomic Force Microscopy (AFM) Analysis

The variation in the thickness of exfoliated BP nanosheets was evaluated by Brucker Dimension Icon atomic force microscope (AFM) in standard tapping mode. The samples were prepared by drop-casting 5μl exfoliated few-layer BP suspension on the silicon wafer and quickly heat dried at 60°C on a hot plate.

Chemical Stability Evaluation of Synthesized BP Nanosheets

Energy Dispersive X-Ray Spectroscopy (EDS) Analysis

EDS elemental mapping and analysis was performed on the exfoliated BP nanosheets with an aberration-corrected JEOL ARM200CF scanning TEM (STEM/TEM) in EDS mode. To evaluate the degree of oxidation, the BP nanosheets stored in deoxygenated water and as exposed to air were compared after 10 days of synthesis. EDS analysis for BP nanosheets stored in deoxygenated water was performed by drop-casting 1 μL of suspension on (LC325-AU) TEM grid and allowed to dry for 10 minutes at room temperature before analysis. Other sample of exfoliated few-layer BP nanosheets was drop casted with 1μl of suspension on (LC300-CU-150) TEM grid and allowed to expose to air for 10 days. EDS analysis was performed at 80 keV incident voltage with 60s of data acquisition time.

Electron Energy Loss Spectroscopy (EELS) Analysis

EELS analysis was performed on exfoliated BP nanosheets stored in deoxygenated water and as exposed to air after 10 days of synthesis using an aberration-corrected JEOL ARM200CF scanning TEM (STEM/TEM). For EELS analysis, high-angle annular dark-field (HAADF) images were acquired in the spherical-aberration corrector STEM mode with a spatial resolution of 1.2 Å at 80 keV incident voltage. For STEM and EELS imaging, convergence angle of 17.8 mrad was used. The collection angle of 90 mrad was used for STEM/HAADF imaging. For EELS, collection semi-angle of 53.4 mrad was used.

Antibacterial Activity of Synthesized BP Nanosheets

In vitro Antibacterial Test – Colony Counting Method

The colony counting method is utilized to evaluate the quantitative bactericidal efficiency of exfoliated BP nanosheets against gram-negative *E. coli* bacteria. Primarily, LB Broth medium and LB Agar plates were prepared as per manufacturer's instructions. The bacteria culture was prepared by inoculating *E. coli* in sterilized LB broth medium and incubating for 12 hours at 37°C under shaking to achieve 10^8 CFU/mL concentration. Further, bacteria control sample without BP nanosheets, bacteria sample with 50 μg/mL of BP nanosheets and with 100 μg/mL of BP nanosheets were incubated for 12 hours at 37°C under shaking. After 12 hours of incubation, respective bacteria cultures were diluted with sterilized water with series of dilutions (10^{-1}, 10^{-2}, 10^{-4} and 10^{-6}). Twenty microliters of each dilution was spread onto LB agar plates which were incubated overnight to evaluate the colony-forming units. The experiments were performed in the triplicates for each dilution. Bactericidal efficiency was calculated with respect to the control bacteria sample without BP nanosheets interaction. The obtained data are expressed as mean ± standard deviation. For each concentration of BP nanosheets, experiments were repeated in the triplicates. All data were statistically analyzed with one-way ANOVA technique. The statistical significance between sample groups was evaluated by the Bonferroni–Holm-corrected method ($p < 0.05$).

Scanning Electron Microscopy (SEM) Analysis of Bacteria

Complementary to TEM studies, to examine the morphological changes that occurred in *E. coli* bacteria upon interaction with 2D BP nanosheets, SEM analysis was performed with

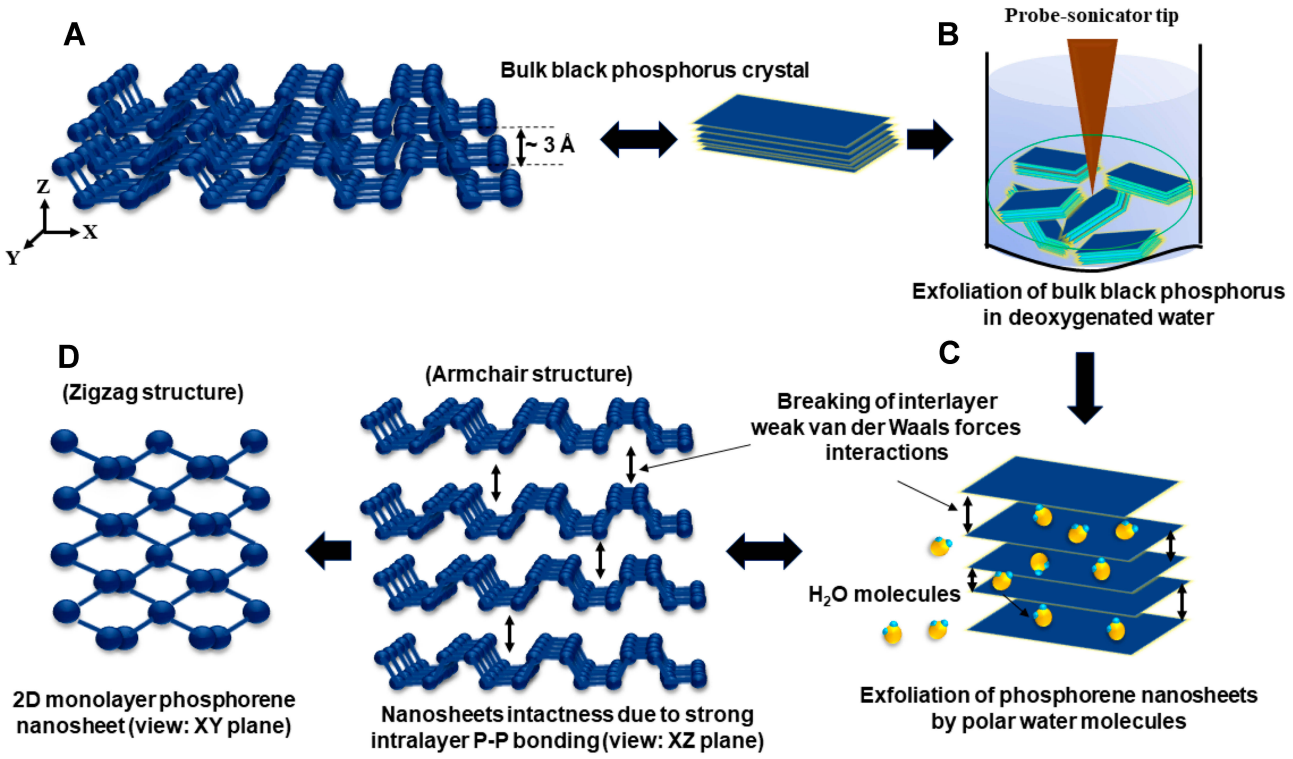

Figure 1 Schematic representation of few-layer BP nanosheet synthesis by liquid exfoliation method. (**A**) Bulk BP crystal made of closely attached 2D phosphorene layers. (**B**) Probe-sonication of BP crystals in the deoxygenated water media in the air-tight container to avoid oxidation. (**C**) Breaking of interlayer weak van der Waals forces by polar water molecules. Ultrasound frequency, probe power, sonication active time and lag time play a critical role in the exfoliation process to achieve ultra-large BP nanosheets. (**D**) As-synthesized exfoliated BP nanosheets viewed at XZ and XY planes.

Abbreviations: BP, black phosphorus; 2D, two dimensional; *E. coli, Escherichia coli*; TEM, transmission electron microscopy, SEM, scanning electron microscopy; AFM, atomic force microscopy; ATR-FTIR, attenuated total reflectance-Fourier-transform infrared spectroscopy; STEM, scanning transmission electron microscopy; HAADF, high angle annular dark field; EDS, energy dispersive X-ray spectroscopy; EELS, electron energy loss spectroscopy; DNA, deoxyribonucleic acid; GO, graphene oxide; rGO, reduced graphene oxide; ROS, reactive oxygen species; MoS_2, molybdenum disulfide; MnO_2, manganese dioxide; IPA, isopropyl alcohol; HMDS, hexamethyldisilazane; NMP, *N*-methyl-2-pyrrolidone; DMSO, dimethyl sulfoxide; N12P, 1-vinyl-2-pyrrolidinone; DMF, *N,N*-dimethylformamide

Raith eLine EBL system equipped with ZEISS SEM column. SEM images were acquired for gold-coated bacteria samples at 10 keV accelerating voltage with 10 mm working distance. SEM samples were prepared by interacting BP nanosheets (100 µg/mL concentration) with *E. coli* bacteria for 3 hours. BP nanosheets-treated bacteria culture was centrifuged at high rpm to obtain the cell pellet, which was rinsed further three times consecutively with PBS. This was followed by cell fixation, which was carried out for 2 hours with 2.5% glutaraldehyde fixative with phosphate buffer solution. Then, cells were again rinsed with PBS and dehydrated with 30%, 50%, 70%, 80%, 95% and twice for 100% ethanol concentrations successively for 10 minutes each. Critical drying step was performed by treating dehydrated bacteria pellet with 50% and 100% hexamethyldisilazane (HMDS) solution as mentioned in earlier published reports.[40] At the end, 20 µL solution of bacterial cell pellet diluted with 100% HMDS was dropped on a glass slide and was allowed to air dry for 24 hours before applying a gold coating of 8 nm thickness.

Ultramicrotome Bacteria TEM Samples' Preparation

To prepare ultramicrotome bacteria TEM samples, primarily bacteria cultures were prepared in sterilized LB Broth by incubating at 37°C for 12 hours. Exfoliated few-layer BP suspension (100 µg/mL) was mixed with bacteria culture and incubated for 6 hours at 37°C. To prepare resin-embedded samples, exfoliated BP-treated and as-cultured controlled bacteria cells were centrifuged at 4000 rpm for 20 minutes. Thereafter, the supernatant was removed, and the collected bacteria pellets were rinsed two times by dispersing in the PBS. Cell fixation was achieved with 2% glutaraldehyde by interacting with the obtained bacteria pellet overnight at 4°C and successively treated with 1% osmium tetroxide for 1 hour. The dehydration was carried out with 30%, 50%, 70%, 80%, 95% and 100% of ethyl alcohol for the duration of 30 minutes for each step. The fixed and dehydrated cell pellet was infiltrated and embedded in 100% resin and placed in embedding mold (Cat. #70907 Dykstra) by maintaining the temperature at 60°C for 48 hours. Bacteria-embedded resin blocks

were sectioned with ultramicrotome (Leica UCT) by using glass knives and diamond knives successively to achieve the section thickness of 100 nm. To analyze the sections with JEOL JEM 1220 TEM (80 KeV), the samples were transferred on a TEM grid (Cat. #EMS200-Cu) and were positively stained with 2% uranyl acetate and 1% lead citrate for 12 minutes and 1 minute, respectively. HAADF-STEM image and EDS line mapping elemental analysis of BP nanosheets-treated damaged *E. coli* bacterium were performed by using an aberration-corrected JEOL ARM200CF scanning TEM (STEM/TEM) operated at 80 KeV.

Results

Characterization of BP Nanosheets

In this section, in order to understand the importance for evaluating the chemical stability of synthesized BP nanosheets, we have briefly introduced the theory and challenges involved in the synthesis of BP nanosheets by the liquid exfoliation route. The molecular level alterations occurring in the BP nanosheets upon oxidation are briefly explained. Further, morphological characterization results of synthesized BP nanosheets with the help of TEM, Raman spectroscopy and AFM techniques and their respective elemental compositional analysis with the help of EDS and EELS techniques are described.

The liquid exfoliation is considered as one of the efficient and facile methods to synthesize few-layer BP nanosheets.[22] For liquid exfoliation, an ideal solvent should be cost-effective, environmentally friendly and efficient in terms of protecting BP nanosheets from oxidation. Moreover, most of the solvents which can synthesize BP nanosheets require post-processing such as transfer of solvent and rinsing to be able to make the BP suitable for biological applications. This increases the possibility of oxidation of phosphorene nanosheets as they form edge and basal surface oxidizes upon being exposed to free O_2 molecules.[41–43] Various studies have been carried out to prove liquid exfoliation efficiency and chemical stability of as-synthesized exfoliated BP nanosheets in mainly organic solvents such as, *N*-methyl-2-pyrrolidone (NMP), dimethyl sulfoxide (DMSO), 1-vinyl-2-pyrrolidinone (N12P), benzaldehyde, isopropyl alcohol (IPA), *N, N*-dimethylformamide (DMF).[42,44] The environmental and biological toxicity of these organic solvents have always been the challenge. The liquid exfoliation method using deoxygenated water as polar solvent to obtain BP nanosheets is a non-toxic, eco-friendly and cost-effective alternative.[23,43,45] Our results show that by tuning process parameters of the liquid exfoliation method, it is possible to synthesize large surface area and chemically stable few-layer BP nanosheets in the deoxygenated water. Liquid exfoliation process works with compression and rarefaction cycles, where the pressure of rarefaction cycle is more responsible for creating transient microbubbles and collapsing of these bubbles generates the instantaneous heat and high local pressure causing the separation of 2D adjacent layers by overcoming van der Waals interactions.[46] Moreover, BP has a tendency to degrade with oxidation upon getting in contact with free oxygen molecules either in air or in water.[22] P_xO_y oxide formation, most likely P_3O_6, P_4O_{10}, is the first stage of BP oxidation which can further react with H_2O to form phosphoric acid (H_3PO_4).[22] The oxidized species of phosphorene may include dangling single (P-OH) and double (P=0) bonds or bridging (P-O-P) bonds.[42,47,48] Considering these attributes we performed chemical stability evaluation of synthesized ultra-large BP nanosheets with the help of EELS and EDS techniques (Figure 2) to ensure BP nanosheets were pristine before treating them with *E. coli* bacteria. We believe quality and initial chemical stability of synthesized BP nanosheets might have played a critical role in exhibiting excellent antibacterial performance, which has been demonstrated by in vitro colony counting method (Figure 3).

The morphological characterization and elemental analysis of synthesized BP nanosheets is represented in Figure 2. Figure 2A shows the low-magnification TEM image of as-synthesized exfoliated few-layer BP nanosheets. The few-layer BP nanosheets possess lateral lengths ranging from 0.5 μm to 4.9 μm (the average length is 2.1μm). Raman scattering was performed to characterize as-synthesized exfoliated few-layer BP (Figure 2B). Raman spectrum shows the characteristic vibrational modes for BP nanosheets. When the incident laser beam is exactly perpendicular to the few-layer exfoliated sheets, only three vibrational modes (out-of-plane mode A_g^1 (~361 cm^{-1}) and in-plane modes B_{2g} (~437 cm^{-1}) and A_g^2 (~466 cm^{-1})) can be detected as represented in Figure 2C.[38,39,43,49] Additionally, Raman spectroscopy confirms the exfoliated few-layer BP nanosheets have maintained the crystalline structure attributed to their characteristic peak positions.[44,50] The integrated intensity ratio of $A_g^1/A_g^2 > 0.2$ can be ascribed with a low oxidation level.[50] AFM analysis to characterize the exfoliated BP thickness variation was performed on randomly selected flakes (Figure 2D). The thickness variation was found to be within 1.1 nm to 8.3 nm wide range.

To investigate the chemical stability of as-synthesized few-layer BP nanosheets, EELS and EDS characterizations were

performed. Figure 2E shows the HAADF-STEM images of the exfoliated few-layer BP as stored in deoxygenated water after 10 days from the day of synthesis and as exposed to ambient room temperature conditions. Respective EELS signals were collected for phosphorus $L_{2,3}$ edge to speculate the presence of the formed oxidation. Local chemical analysis of EELS signal shows signature peaks at ~130 eV and ~136 eV which can be attributed to pristine BP nanosheets and oxidized BP nanosheets (P_xO_y) states, respectively. The EELS signal for as-synthesized exfoliated BP nanosheets stored in deoxygenated water, even after 10 days, confirms the absence of P_xO_y peak. Figure 2F and G shows the complementary EDS characterization along with elemental mapping performed on the exfoliated few-layer BP as stored in deoxygenated water after 10 days from the day of synthesis and exposed to ambient room temperature conditions. The EDS spectroscopy clearly indicates the absence of oxygen K-edge at 0.5 keV for the exfoliated BP stored in deoxygenated water. Additionally, EDS layered map gives the elemental composition for a specific region of BP nanosheet indicating the presence of oxygen for the BP nanosheets exposed to ambient air conditions. Detection of other elements such as carbon (C), copper (Cu), and gold (Au) are due to lacey carbon-coated gold and copper TEM grids.

Antibacterial Activity of BP Nanosheets

In vitro Antibacterial Colony Counting Assay

The antibacterial activity of as-synthesized BP nanosheets was assessed against Gram-negative *E. coli* bacteria. The bactericidal efficiency was evaluated by the LB-agar colony counting method (10^8 CFU/mL, 20 µL bacterial suspension). In Figure 3A, colony forming units (CFU) represents untreated *E. coli* considered as a base control. After 12 hours of treatment with few-layer BP nanosheets, significant reduction in CFU can be observed in Figure 3B and C, which was ~87% bactericidal efficiency with 50 µg/mL and ~95% bactericidal efficiency at 100 µg/mL BP nanosheet concentrations, respectively (represented in Figure 3D). Earlier BP nanosheets bactericidal efficiency was reported as ~90% (at 50 µg/mL BP nanosheet concentration) and ~99% (at 100 µg/mL BP nanosheet concentration) after 6 hours of treatment, although which was reduced subsequently after 12 hours progressive interaction attributing to the recovery of temporarily damaged *E. coli* bacterial cell membrane.[23] BP nanosheets upon 3 minutes of irradiation at 160 µg/mL concentration can irradiate ~99.2% *E. coli* bacteria within 4 hours.[18] Our observations indicate the bactericidal efficiency was maintained as high as around 95% even after 12 hours of treatment. Figure 3D indicates that the statistical significance exists among the CFU data groups as evaluated with one-way ANOVA technique followed by the Bonferroni–Holm's correction for $p < 0.05$. The observed remarkable bactericidal efficiency can be possibly attributed with the chemical stability and physical interaction of ultra-large (micron scale) lateral size of few-layer BP nanosheets. Further iterative studies are required in determining the minimum inhibition concentration (MIC) and minimum bactericidal concentration (MBC) of synthesized BP nanosheets which can promote their utilization as advanced antibacterial platforms in the biomedical field. To evaluate the morphological changes occurred during the intermediate stages of bacterial cell rupture, the cultured *E. coli* cells were treated with BP nanosheets only for 3 hours for SEM and TEM studies.

Scanning Electron Microscopy Analysis of *E. coli* Bacteria Treated with BP Nanosheets

Figure 4A shows the SEM micrographs of untreated *E. coli* bacteria confirming smooth and intact surfaces. After incubating bacteria with BP nanosheets with 100 µg/mL concentration for 3 hours, significant changes are observed in the bacterial cell morphology which can be observed from Figure 4. Upon interacting with BP nanosheets bacteria seem to lose structural integrity and surface intactness. In Figure 4B–D, distorted bacterial cell structure with excessive membrane damage and pores can be observed which could be possibly due to the physical damage caused by BP nanosheets. It also shows shrinkage of bacterium more likely caused due to collapsed of internal structure.[51] Similar trends of lost bacterial cell integrity were observed in TEM analysis which are discussed in the following section, Figure 4D shows punctured bacterium which could occur either due to oxidative stress on the bacterial cell membrane or physical membrane damage caused by BP nanosheets.[23] Reduction in the cell membrane components is also confirmed with ATR-FTIR chemical analysis of damaged bacterial cells (Figure S2). Further iterative studies could be interesting to perform for evaluating the bacterial cell membrane damage caused by BP nanosheets at lower dose rates and at varying interaction time periods.

Transmission Electron Microscopy Analysis of *E. coli* Bacteria Treated with BP Nanosheets

To demonstrate the interaction of BP nanosheets with *E. coli* bacteria at nanoscale and to capture various events of cellular damage and bacterial cells internal modifications, TEM studies were performed. Figure 5 shows the colored representative TEM micrographs of various events of *E.coli* bacterial cell damage as upon treating with BP nanosheets. Figure S1

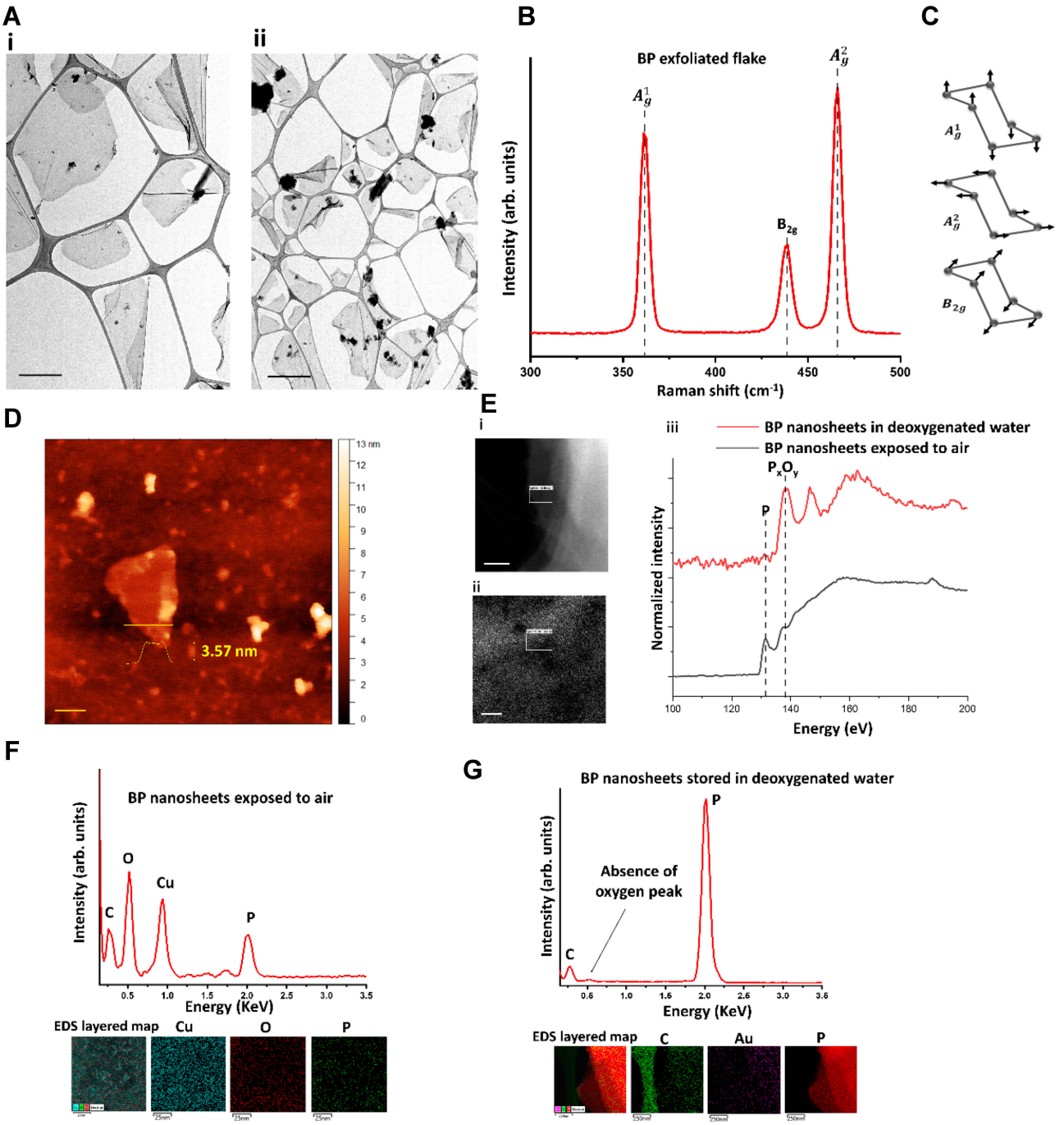

Figure 2 Morphological characterization and elemental analysis of BP nanosheets. (**A**) Low-magnification TEM images of exfoliated BP ultra-large nanosheets. In image i, the scale bar represents 1 μm, and in image ii, the scale bar is 2 μm. (**B**) Raman spectra of exfoliated BP showing characteristic peaks of BP. (**C**) Representative schematic of out-of-plane and in-plane vibrational modes for BP – Raman analysis. (**D**) AFM analysis to confirm the exfoliated BP nanosheets thickness variation (scale bar is 50 nm). (**E**) EELS analysis: i. The high-angle annular dark-field (HAADF)-STEM image of BP flake exposed to air, acquired at 80 kV (scale bar is 20 nm). ii. The HAADF-STEM image of BP flake in deoxygenated water (scale bar is 0.2 μm). iii. The EELS spectra corresponding to the selected area in i and ii shows the P-$L_{2,3}$ edge of bulk BP and BP nanosheet confirming the BP nanosheets stored in the deoxygenated water were not oxidized. (**F**) The EDS analysis of BP flake exposed to air along with elemental mapping confirming the presence of oxygen (scale bar is 25 nm). (**G**) The EDS analysis of BP flake stored in deoxygenated water along with elemental mapping confirming the absence of oxygen (scale bar is 250 nm).

represents respective TEM micrographs of Figure 5. Figure 5A shows the morphology of healthy *E. coli* bacteria untreated with BP nanosheets. We can observe the integrity of the cell envelope, where the cytoplasm is intact with the bacterial cell membrane. Also, thick cell wall with higher lipid bilayer density can be observed. In Figure 5A, the uniform electron density can be observed in the untreated bacteria, assuring the cells are functioning normally without any external

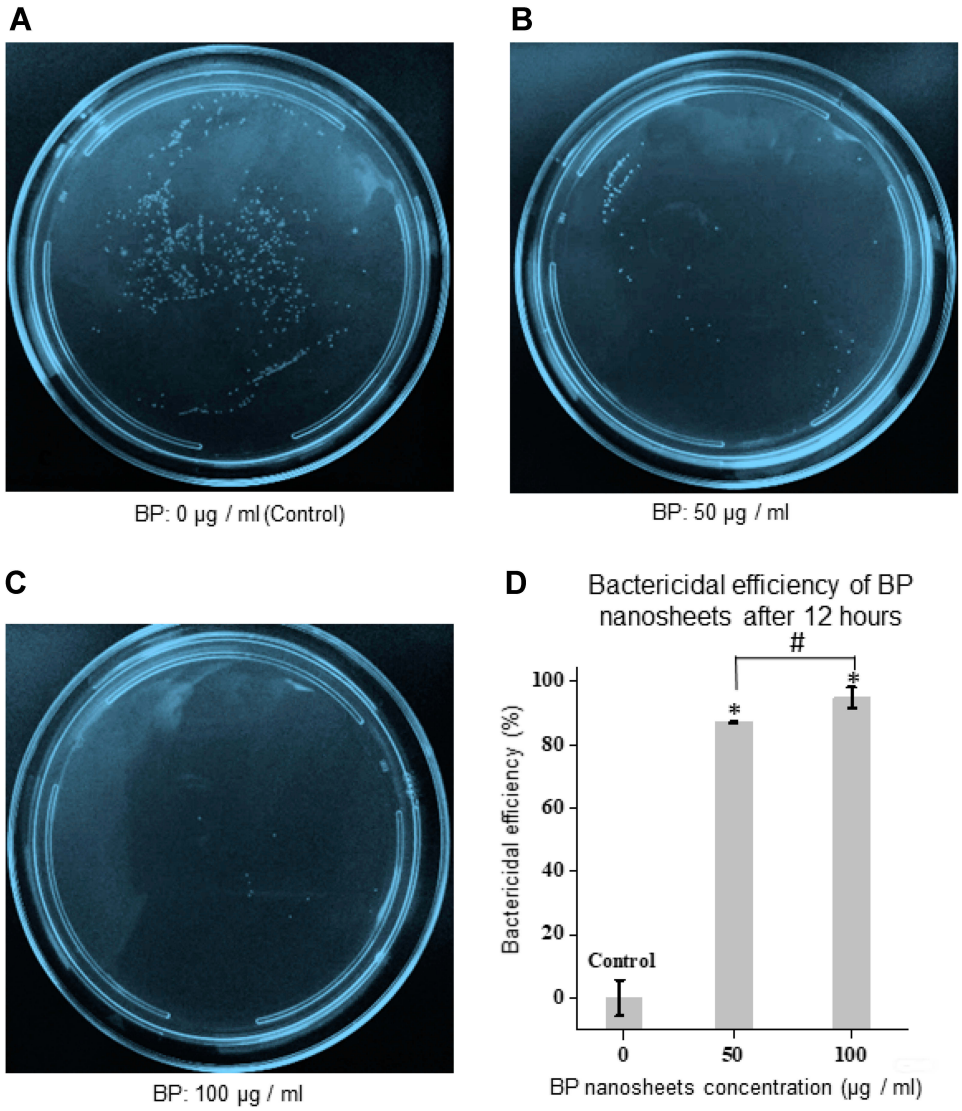

Figure 3 In vitro antibacterial test results of BP nanosheets against *E. coli* bacteria evaluated by colony counting method after 12 hours of treatment. (**A**) The colony-forming units of control sample without any BP nanosheets. (**B**) The colony-forming units with the treatment of 50 µg/mL of exfoliated BP nanosheets. (**C**) The colony-forming units with the treatment of 100 µg/mL of exfoliated BP nanosheets. (**D**) Bactericidal efficiency of BP nanosheets at different concentrations. The error bars represent ± standard deviation for n = 3. *, $p < 0.05$ evaluated as statistically significant for 50 µg/mL and 100 µg/mL BP nanosheet concentration as compared with control (0 µg/mL) sample after Bonferroni–Holm's correction. #, $P < 0.05$ evaluated as statistically significant between 50 µg/mL and 100 µg/mL BP nanosheet concentration after Bonferroni–Holm's correction.

environmental disturbances. The electron-light area can be attributed to DNA molecules that are randomly distributed in overall different regions of prokaryotic cells.[52] TEM micrographs (from Figure 5B-F) indicate the significant changes that occurred in the bacterial cell morphology after interacting with the exfoliated BP nanosheets. The morphological change for the loss of *E. coli* cell integrity is very similar to the TEM micrographs representing *E. coli* bacteria after treating with silver ions.[52] In Figure 5B, the arrows clearly show the cytoplasmic leakage and the disruption of cell wall that resulted in the lost cellular integrity.[53,54] In Figure 5C, an arrow indicates the electron-light region in the center where the quenched DNA structure can be observed, which shows resemblance with the results indicating antibacterial activity of silver ions.[52] The accumulation of cytoplasm in the periplasmic space can occur due to the osmotic imbalance caused by the cell wall damage.[54] In Figure 5F, the arrows indicate the large electron-light areas concentrated at the specific region of the BP-treated bacterial cell indicating the lost cellular integrity as compared with the healthy untreated bacterium as seen in Figure 5A. The detachment of the cytoplasmic membrane from the bacterium cell wall and damaged bacterial cell wall can be clearly observed. The separation of cytoplasmic membrane from the cell wall confirms the malfunctioning and damage caused to

bacterium after interacting with exfoliated few-layer BP nanosheets. The similar separation of cytoplasmic membrane from the cell wall can be observed in Figure 5B and 5E. In Figure 5E, the significantly distorted bacterial cell membrane is observed. Similar distorted bacterial cell morphology can be observed in SEM micrographs (Figure 4C). The reduced phospholipids density of bacterial cells can be confirmed by comparing that for the untreated *E. coli* bacterium in Figure 5A and B P-treated *E. coli* bacterium in Figure 5D. The TEM observation of reduced phospholipids density is similar to that of Tu et al's who reported the damage caused by graphene nanosheets to *E.coli* bacterial cell membrane.[55]

Further, the HAADF-STEM micrograph and EDS elemental line mapping of the damaged bacterial cell upon treating with BP nanosheets can be observed in Figure 6 indicating the concentration gradient of phosphorus, chlorine, sulfur and calcium elements. The increased concentration of these elements outside the cell membrane confirms the lost cellular integrity and the leakage of cytoplasmic components. Figure 6C shows the concentrated cytoplasmic region at the center indicating the phosphorus-rich region. The successive surrounding central region indicates the increased concentration of sulfur as observed in Figure 6E. Figure 6D shows the gradual increase of the concentration of chlorine ions towards outside of the bacterial cell membrane. In Figure 6E highest concentration of calcium ions can be observed outside the bacterial cell membrane. More statistical analysis would be needed to further study the parameters affecting the interaction of BP nanosheets with different classes of bacteria.

Discussion

Antibacterial Activity of BP Nanosheets

The cell wall of Gram-negative *E. coli* bacteria comprises three layers, such as, cytoplasmic inner membrane layer comprising lipid-proteins, outer membrane containing lipopolysaccharides and proteins and intermediate thin (~7 nm thickness) rigid peptidoglycan mesh located in the periplasmic space.[56] Peptidoglycan layer comprising polymeric chains of *N*-acetylmuramic acid and *N*-acetylglucosamine linked with peptides is responsible for the rigidity and the cell membrane integrity.[9,52] BP nanosheets can cause physical damage to the cell wall by triggering the intracellular periplasmic and cytoplasmic leakage. Similar observations of physical damage to cell membrane by nano-knives like behavior of 2D nanomaterials penetrating the cell membrane were noted by Alimohammadi et al[16] for manganese dioxide (MnO_2)

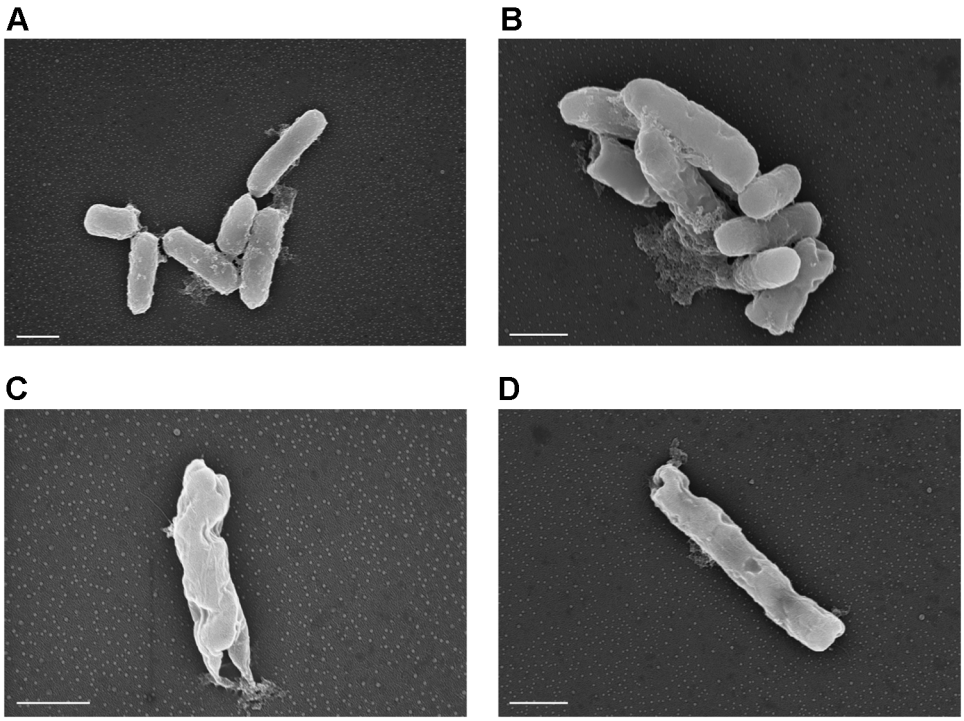

Figure 4 SEM observations of morphology changes in *E. coli* bacteria treated with BP nanosheets (100 μg/mL concentration) for 3 hours. (**A**) Untreated *E. coli* bacteria confirming smooth surface morphology. (**B**) Damaged bacteria surface morphology after treating with BP nanosheets. (**C**) Distorted bacterium indicating lost cellular integrity. (**D**) Damaged bacterium cell wall indicating punctured areas of cell membrane (scale bars are 1 μm).

nanosheets and by Pham et al[57] for graphene nanosheets. Xiong et al[23] have shown the intracellular ROS generation tendency and the reduction in the cell membrane components caused by BP nanosheets. As reported,[52,58–60] UV irradiated ultrathin BP nanosheets possess high anisotropic hole mobility and tunable semiconductor bandgap, which can mainly generate singlet oxygen and superoxide radical as ROS, which possibly can generate oxidative stress and can cause damage to bacterial cell essential macromolecules such as DNA, RNA, proteins and membrane lipids.[61,62] Figure 6 shows the distribution of diagnostic ions across the damaged bacterium upon interacting with BP nanosheets. HAADF-STEM image of *E. coli* highlights the agglomerated cellular components in the center which are rich in phosphorus contents. The origin of phosphorus in the central part of the bacterium is more likely to be associated with quenched DNA molecules and possibly phosphorylated proteins.[52,63] The similar structural resemblance of the quenched DNA molecules can be referred in Figure 5C. The surrounding central area around phosphorus content is rich in sulfur as indicated in Figure 6E. The block element sulfur is mainly associated with proteins found in cysteine and methionine amino acids.[63] The conglomeration of sulfur ions surrounding the phosphorus region can be attributed with the DNA protective cellular function with the help of proteins.[52] Chlorine ions are responsible for cellular homeostasis and calcium ions are utilized for cellular communication and cofactors in metabolisms.[63] The events of agglomerated DNA molecules lose their replication ability, and the release of phosphorus, chlorine, sulfur and calcium diagnostic ions due to disrupted cell membrane permeability is related to the lost cellular metabolism.[52,63] The leakage of cytoplasmic cellular components can be confirmed with TEM micrographs in Figure 5. The events of BP nanosheets interacting with bacteria cell membrane can be observed in Figure 5E. The reduction in the bacterial cell wall components is in line with the ATR-FTIR results (Figure S2). Reduction in the respective intensities in $–CH_2$ and –CH bands indicates changes in the lipid

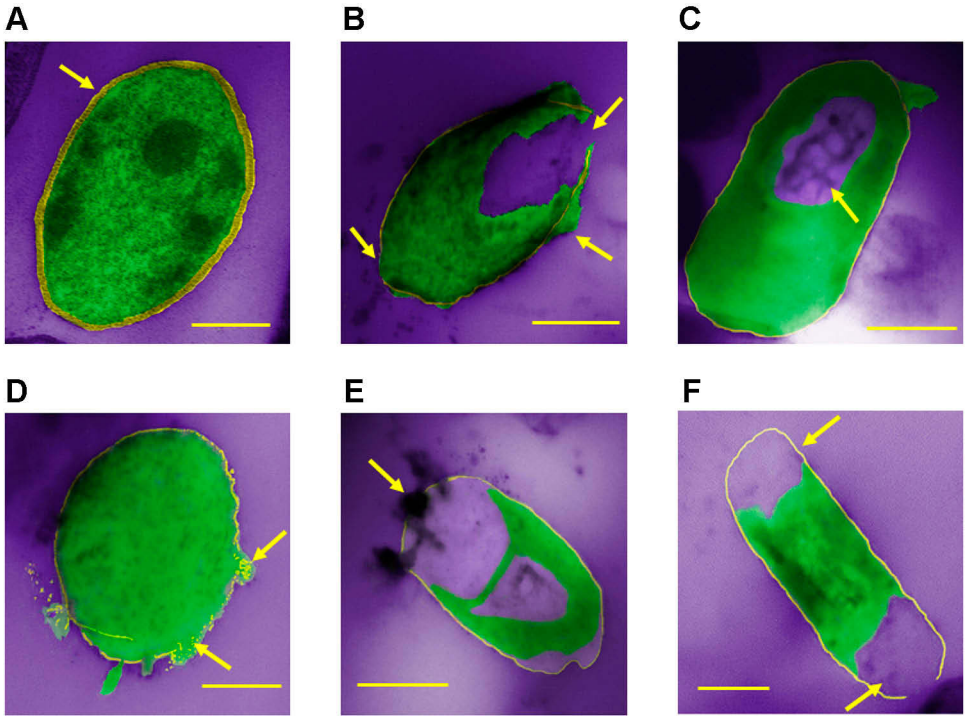

Figure 5 Colored representative TEM micrographs of damaged *E. coli* bacteria upon treating with exfoliated BP nanosheets for 3 hours. (Green, cell medium; yellow, bacterial cell wall; violet, background empty region.) (**A**) Internal cell structure of untreated *E. coli* bacterium – control sample (scale bar is 200 nm). An arrow indicates the intactness of the bacterial cell wall with the cytoplasm. (**B**) Ruptured cell membrane and the event of cytoplasmic leakage from the cell membrane (scale bar is 500 nm). The arrows show the events of the cytoplasmic leakage and the disruption of the bacterial cell wall. (**C**) Central large electron-light area indicating accumulation of DNA molecules confirming disturbed cellular metabolism (scale bar is 400 nm). An arrow indicates the electron-light region in the center of the bacterial cell. (**D**) Reduced density of phospholipids upon interacting with BP nanosheets (scale bar is 200 nm). The arrows indicate the disintegrated phospholipid layer. (**E**) The event of BP nanosheets interacting with cell membrane and detached cytoplasm from the cell membrane (scale bar is 500 nm). An arrow indicates the BP nanosheets attached to the bacterium. (**F**) Ruptured cell wall and separation of cytoplasm from the cell wall (scale bar is 500 nm). The arrows indicate the regions of the lost cellular integrity.

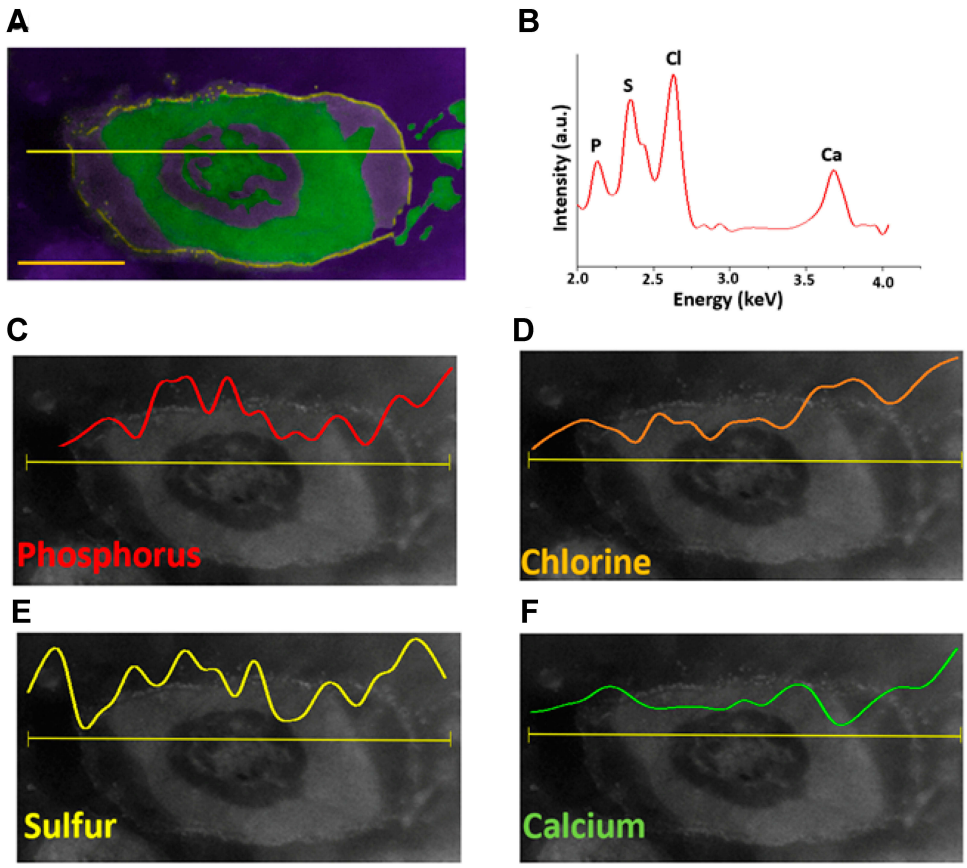

Figure 6 HAADF-STEM images and EDS elemental line mapping of damaged *E. coli* bacterium upon treating with BP nanosheets for 3 hours. (**A**) Colored representative HAADF-STEM image of damaged *E. coli* bacterium. Green, cell medium; yellow, bacterial cell wall; violet, background empty region (scale bar is 500 nm). (**B**) EDS spectrum of damaged *E. coli* bacterium confirming the presence of phosphorus (P), sulfur (S), chlorine (Cl) and calcium (Ca) elements. (**C**) EDS elemental line map indicating the concentration of P across the damaged *E. coli* bacterium. (**D**) EDS elemental line map indicating the concentration of Cl across the damaged *E. coli* bacterium. (**E**) EDS elemental line map indicating the concentration of S across the damaged *E. coli* bacterium. (**F**) EDS elemental line map indicating the concentration of Ca across the damaged *E. coli* bacterium. (The horizontal yellow line across bacterium represents elemental line scan region.)

layer fluidity in the bacterial cell wall which can be interpreted as bacterial lysis and leakage of the cytoplasm from increased membrane permeability.[64,65] The leakage of cytoplasm and reduced band intensities for 2924 cm^{-1} and 2853 cm^{-1} wavenumbers can be associated with the membrane damage caused by BP nanosheets.[66,67] The singlet oxygen generation ability of BP nanosheets can be accounted as the dominating factor to cause damage to the bacterial cell membrane integrity by oxidizing membrane lipids.[61] These results are in accordance with the lipid peroxidation damage of the bacterial cell membrane caused by BP quantum dots.[68] The events of the reduced density of lipid bilayer, the separation of cytoplasmic membrane from the cell wall, the ruptured cell membrane observed in TEM micrographs confirm the lost cellular integrity upon treating with BP nanosheets, which is accordance with the results evaluated from the HAADF-STEM image and EDS elemental line mapping of damaged *E. coli* bacterium. Future efforts should consider the study of how the size of BP nanosheets would affect the interaction mechanisms with the bacteria surfaces. It would be also fascinating to expand on the in-situ liquid TEM studiesc,d,e for unveiling the dynamic antimicrobial events of BP nanosheets.[69,70,71]

Conclusions

We report the nanoscale TEM observations of morphological changes that occurred in *E. coli* bacteria upon interacting with ultra-large BP nanosheets. Chemical stability of ultra-large BP nanosheets synthesized in deoxygenated water was confirmed with EDS and EELS characterization techniques with the absence of oxygen peak. The colony-forming assay confirms the bactericidal efficiency of ultra-large chemically stable BP nanosheets to be ~95%. TEM micrographs show the various events of *E. coli* cell membrane damage and the loss of cellular integrity. These events include the BP nanosheets interacting

with the bacterial cell wall and the cytoplasmic leakage, detachment of cytoplasm from the cell membrane, distorted bacterium morphology, reduced density of lipid bilayer and agglomerated DNA structure leading to the loss of cellular metabolism. The lost cellular integrity, the disrupted membrane permeability and the loss of cytoplasmic and cell membrane components are confirmed by analyzing the presence of diagnostic phosphorus, sulfur, chlorine and calcium ions evaluated with the EDS elemental line mapping of HAADF-STEM image of the damaged bacterium. SEM micrographs of distorted bacterial cells upon treating with BP nanosheets are in line with the findings obtained from TEM studies.

Acknowledgments

This work was supported by the National Science Foundation (NSF) under EArly concept Grants for Exploratory Research (EAGER) program (Award Number: 1803693). R. Shahbazian-Yassar acknowledges the financial support from NSF award DMR-1710049.

Disclosure

The authors report no conflicts of interest in this work.

References

1. Germe T, Voros J, Jeannot F, et al. A new class of antibacterials, the imidazopyrazinones, reveal structural transitions involved in DNA gyrase poisoning and mechanisms of resistance. *Nucleic Acids Res*. 2018;46(8):4114–4128. doi:10.1093/nar/gky181
2. Gupta A, Mumtaz S, Li CH, Hussain I, Rotello VM. Combatting antibiotic-resistant bacteria using nanomaterials. *Chem Soc Rev*. 2019;48(2):415–427. doi:10.1039/C7CS00748E
3. Roy R, Tiwari M, Donelli G, Tiwari V. Strategies for combating bacterial biofilms: a focus on anti-biofilm agents and their mechanisms of action. *Virulence*. 2018;9(1):522–554. doi:10.1080/21505594.2017.1313372
4. Blair JM, Webber MA, Baylay AJ, Ogbolu DO, Piddock LJ. Molecular mechanisms of antibiotic resistance. *Nat Rev Microbiol*. 2015;13(1):42–51. doi:10.1038/nrmicro3380
5. Levy SB, Marshall B. Antibacterial resistance worldwide: causes, challenges and responses. *Nat Med*. 2004;10(12 Suppl):S122–S129. doi:10.1038/nm1145
6. Xu JW, Yao K, Xu ZK. Nanomaterials with a photothermal effect for antibacterial activities: an overview. *Nanoscale*. 2019;11(18):8680–8691. doi:10.1039/C9NR01833F
7. Phakatkar AH, Shirdar MR, Qi M-l, et al. Novel PMMA bone cement nanocomposites containing magnesium phosphate nanosheets and hydroxyapatite nanofibers. *Materials Science and Engineering: C*. 2020;109:110497.
8. Qi M-l, Huang Z, Phakatkar A, et al. Facile hydrothermal synthesis of antibacterial multi-layered hydroxyapatite nanostructures with superior flexibility. *CrystEngComm*. 2018;20(9):1304–1312.
9. Alimohammadi F, Sharifian GM, Attanayake NH, et al. Antimicrobial properties of 2D MnO2 and MoS2 nanomaterials vertically aligned on graphene materials and Ti3C2 MXene. *Langmuir*. 2018;34(24):7192–7200. doi:10.1021/acs.langmuir.8b00262
10. Liu C, Kong D, Hsu P-C, et al. Rapid water disinfection using vertically aligned MoS2 nanofilms and visible light. *Nat Nanotechnol*. 2016;11(12):1098–1104. doi:10.1038/nnano.2016.138
11. Zou F, Zhou H, Jeong DY, et al. Wrinkled surface-mediated antibacterial activity of graphene oxide nanosheets. *ACS Appl Mater Interfaces*. 2017;9(2):1343–1351. doi:10.1021/acsami.6b15085
12. Wang G, Feng W, Zeng X, et al. Highly recoverable TiO2-GO nanocomposites for stormwater disinfection. *Water Res*. 2016;94:363–370. doi:10.1016/j.watres.2016.02.067
13. Ge C, Fang G, Shen X, et al. Facet energy versus enzyme-like activities: the unexpected protection of palladium nanocrystals against oxidative damage. *ACS Nano*. 2016;10(11):10436–10445. doi:10.1021/acsnano.6b06297
14. Maisch T. Resistance in antimicrobial photodynamic inactivation of bacteria. *Photochem Photobiol Sci*. 2015;14(8):1518–1526. doi:10.1039/C5PP00037H
15. Burns JM, Cooper WJ, Ferry JL, et al. Methods for reactive oxygen species (ROS) detection in aqueous environments. *Aquat Sci*. 2012;74(4):683–734.
16. Sabbahi S, Alouini Z, Jemli M, Boudabbous A. The role of reactive oxygen species in Staphylococcus aureus photoinactivation by methylene blue. *Water Sci Technol*. 2008;58(5):1047–1054. doi:10.2166/wst.2008.471
17. Redmond RW, Kochevar IE. Spatially resolved cellular responses to singlet oxygen. *Photochem Photobiol*. 2006;82(5):1178–1187. doi:10.1562/2006-04-14-IR-874
18. Sun Z, Zhang Y, Yu H, et al. New solvent-stabilized few-layer black phosphorus for antibacterial applications. *Nanoscale*. 2018;10(26):12543–12553.
19. Bagheri S, Mansouri N, Aghaie E. Phosphorene: a new competitor for graphene. *Int J Hydrogen Energy*. 2016;41(7):4085–4095.
20. Tao W, Zhu X, Yu X, et al. Black phosphorus nanosheets as a robust delivery platform for cancer theranostics. *Adv Mater*. 2017;29:1. doi:10.1002/adma.201700681
21. Brent JR, Savjani N, Lewis EA, Haigh SJ, Lewis DJ, O'Brien P. Production of few-layer phosphorene by liquid exfoliation of black phosphorus. *Chem Commun (Camb)*. 2014;50(87):13338–13341. doi:10.1039/C4CC05752J
22. Tan L, Li J, Liu X, et al. In situ disinfection through photoinspired radical oxygen species storage and thermal-triggered release from black phosphorous with strengthened chemical stability. *Small*. 2018;14(9):9.
23. Xiong Z, Zhang X, Zhang S, et al. Bacterial toxicity of exfoliated black phosphorus nanosheets. *Ecotoxicol Environ Saf*. 2018;161:507–514. doi:10.1016/j.ecoenv.2018.06.008
24. Zhang X, Zhang Z, Zhang S, et al. Size effect on the cytotoxicity of layered black phosphorus and underlying mechanisms. *Small*. 2017;13:32.
25. Song SJ, Shin YC, Lee HU, Kim B, Han DW, Lim D. Dose and time-dependent cytotoxicity of layered black phosphorus in fibroblastic cells. *Nanomaterials (Basel)*. 2018;8:6. doi:10.3390/nano8060408
26. Lee HU, Park SY, Lee SC, et al. Black Phosphorus (BP) nanodots for potential biomedical applications. *Small*. 2016;12(2):214–219. doi:10.1002/smll.201502756
27. Chen W, Ouyang J, Liu H, et al. Black phosphorus nanosheet-based drug delivery system for synergistic photodynamic/photothermal/chemotherapy of cancer. *Adv Mater*. 2017;29:5.
28. Engel M, Steiner M, Avouris P. Black phosphorus photodetector for multispectral, high-resolution imaging. *Nano Lett*. 2014;14(11):6414–6417. doi:10.1021/nl502928y
29. Fu H, Li Z, Xie H, et al. Different-sized black phosphorus nanosheets with good cytocompatibility and high photothermal performance. *RSC Adv*. 2017;7(24):14618–14624. doi:10.1039/C7RA00160F
30. Serrano-Ruiz M, Caporali M, Ienco A, Piazza V, Heun S, Peruzzini M. The role of water in the preparation and stabilization of high-quality phosphorene flakes. *Adv Mater Interfaces*. 2016;3(3):1500441. doi:10.1002/admi.201500441

31. Ouellette RJ, Rawn JD. *Organic Chemistry: Structure, Mechanism, and Synthesis*. Saint Louis, USA: Elsevier; 2014.
32. Lazar P, Otyepkova E, Pykal M, Cepe K, Otyepka M. Role of the puckered anisotropic surface in the surface and adsorption properties of black phosphorus. *Nanoscale*. 2018;10(19):8979–8988. doi:10.1039/C8NR00329G
33. Qiu M, Ren WX, Jeong T, et al. Omnipotent phosphorene: a next-generation, two-dimensional nanoplatform for multidisciplinary biomedical applications. *Chem Soc Rev*. 2018;47(15):5588–5601. doi:10.1039/C8CS00342D
34. Zhang W, Huynh T, Xiu P, et al. Revealing the importance of surface morphology of nanomaterials to biological responses: adsorption of the villin headpiece onto graphene and phosphorene. *Carbon*. 2015;94:895–902. doi:10.1016/j.carbon.2015.07.075
35. Peng J, Lai Y, Chen Y, Xu J, Sun L, Weng J. Sensitive detection of carcinoembryonic antigen using stability-limited few-layer black phosphorus as an electron donor and a reservoir. *Small*. 2017;13(15):15. doi:10.1002/smll.201603589
36. Ge Y, Camarada MB, Xu L, et al. A highly stable black phosphorene nanocomposite for voltammetric detection of clenbuterol. *Mikrochim Acta*. 2018;185(12):566. doi:10.1007/s00604-018-3084-z
37. Kumar V, Brent JR, Shorie M, et al. Nanostructured aptamer-functionalized black phosphorus sensing platform for label-free detection of myoglobin, a cardiovascular disease biomarker. *ACS Appl Mater Interfaces*. 2016;8(35):22860–22868. doi:10.1021/acsami.6b06488
38. Guo Z, Zhang H, Lu S, et al. From black phosphorus to phosphorene: basic solvent exfoliation, evolution of raman scattering, and applications to ultrafast photonics. *Adv Funct Mater*. 2015;25(45):6996–7002. doi:10.1002/adfm.201502902
39. Yasaei P, Kumar B, Foroozan T, et al. High-quality black phosphorus atomic layers by liquid-phase exfoliation. *Adv Mater*. 2015;27(11):1887–1892. doi:10.1002/adma.201405150
40. Hazrin-Chong NH, Manefield M. An alternative SEM drying method using hexamethyldisilazane (HMDS) for microbial cell attachment studies on sub-bituminous coal. *J Microbiol Methods*. 2012;90(2):96–99. doi:10.1016/j.mimet.2012.04.014
41. Ziletti A, Carvalho A, Campbell DK, Coker DF, Castro Neto AH. Oxygen defects in phosphorene. *Phys Rev Lett*. 2015;114(4):046801. doi:10.1103/PhysRevLett.114.046801
42. Kuntz KL, Wells RA, Hu J, et al. Control of surface and edge oxidation on phosphorene. *ACS Appl Mater Interfaces*. 2017;9(10):9126–9135. doi:10.1021/acsami.6b16111
43. Kang J, Wells SA, Wood JD, et al. Stable aqueous dispersions of optically and electronically active phosphorene. *Proc Natl Acad Sci U S A*. 2016;113(42):11688–11693. doi:10.1073/pnas.1602215113
44. Lei W, Liu G, Zhang J, Liu M. Black phosphorus nanostructures: recent advances in hybridization, doping and functionalization. *Chem Soc Rev*. 2017;46(12):3492–3509. doi:10.1039/C7CS00021A
45. Pan S, He J, Wang C, Zuo Y. Exfoliation of two-dimensional phosphorene sheets with enhanced photocatalytic activity under simulated sunlight. *Mater Lett*. 2018;212:311–314. doi:10.1016/j.matlet.2017.10.090
46. Tao H, Zhang Y, Gao Y, Sun Z, Yan C, Texter J. Scalable exfoliation and dispersion of two-dimensional materials - an update. *Phys Chem Chem Phys*. 2017;19(2):921–960. doi:10.1039/C6CP06813H
47. Wood JD, Wells SA, Jariwala D, et al. Effective passivation of exfoliated black phosphorus transistors against ambient degradation. *Nano Lett*. 2014;14(12):6964–6970. doi:10.1021/nl5032293
48. Yang T, Dong B, Wang J, et al. Interpreting core-level spectra of oxidizing phosphorene: theory and experiment. *Phys Rev B*. 2015;92(12):12. doi:10.1103/PhysRevB.92.125412
49. Lu W, Nan H, Hong J, et al. Plasma-assisted fabrication of monolayer phosphorene and its Raman characterization. *Nano Res*. 2014;7(6):853–859. doi:10.1007/s12274-014-0446-7
50. Favron A, Gaufres E, Fossard F, et al. Photooxidation and quantum confinement effects in exfoliated black phosphorus. *Nat Mater*. 2015;14(8):826–832. doi:10.1038/nmat4299
51. Valentini F, Calcaterra A, Ruggiero V, et al. Functionalized graphene derivatives: antibacterial properties and cytotoxicity. *J Nanomater*. 2019;2019.
52. Feng QL, Wu J, Chen GQ, Cui FZ, Kim TN, Kim JO. A mechanistic study of the antibacterial effect of silver ions on Escherichia coli and Staphylococcus aureus. *J Biomed Mater Res*. 2000;52(4):662–668. doi:10.1002/1097-4636(20001215)52:4<662::AID-JBM10>3.0.CO;2-3
53. Li A, Lee PY, Ho B, Ding JL, Lim CT. Atomic force microscopy study of the antimicrobial action of Sushi peptides on Gram negative bacteria. *Biochim Biophys Acta*. 2007;1768(3):411–418. doi:10.1016/j.bbamem.2006.12.010
54. Hartmann M, Berditsch M, Hawecker J, Ardakani MF, Gerthsen D, Ulrich AS. Damage of the bacterial cell envelope by antimicrobial peptides gramicidin S and PGLa as revealed by transmission and scanning electron microscopy. *Antimicrob Agents Chemother*. 2010;54(8):3132–3142. doi:10.1128/AAC.00124-10
55. Tu Y, Lv M, Xiu P, et al. Destructive extraction of phospholipids from Escherichia coli membranes by graphene nanosheets. *Nat Nanotechnol*. 2013;8(8):594. doi:10.1038/nnano.2013.125
56. Godlewska R, Wisniewska K, Pietras Z, Jagusztyn-Krynicka EK. Peptidoglycan-associated lipoprotein (Pal) of Gram-negative bacteria: function, structure, role in pathogenesis and potential application in immunoprophylaxis. *FEMS Microbiol Lett*. 2009;298(1):1–11. doi:10.1111/j.1574-6968.2009.01659.x
57. Pham VT, Truong VK, Quinn MD, et al. Graphene induces formation of pores that kill spherical and rod-shaped bacteria. *ACS Nano*. 2015;9(8):8458–8467. doi:10.1021/acsnano.5b03368
58. Wang J, Tao W, Chen X, Farokhzad OC, Liu G. Emerging advances in nanotheranostics with intelligent bioresponsive systems. *Theranostics*. 2017;7(16):3915. doi:10.7150/thno.21317
59. Bagheri S, Mansouri N, Aghaie E. Phosphorene: a new competitor for graphene. *Int J Hydrogen Energy*. 2016;41(7):4085–4095.
60. Sun Z, Zhang Y, Yu H, et al. New solvent-stabilized few-layer black phosphorus for antibacterial applications. *Nanoscale*. 2018;10(26):12543–12553.
61. Tan L, Li J, Liu X, et al. In situ disinfection through photoinspired radical oxygen species storage and thermal-triggered release from black phosphorous with strengthened chemical stability. *Small*. 2018;14(9):1703197.
62. Tao Y, Ju E, Ren J, Qu X. Bifunctionalized mesoporous silica-supported gold nanoparticles: intrinsic oxidase and peroxidase catalytic activities for antibacterial applications. *Adv Mater*. 2015;27(6):1097–1104. doi:10.1002/adma.201405105
63. Liu JL, Luo Z, Bashir S. A progressive approach on inactivation of bacteria using silver–titania nanoparticles. *Biomater Sci*. 2013;1(2):194–201. doi:10.1039/C2BM00010E
64. Fang J, Wiesner M, Dong J, Alvarez P. Effect of a fullerene water suspension on bacterial phospholipids and membrane phase behavior. *Environ Sci Technol*. 2007;41(7):2636–2642. doi:10.1021/es062181w
65. Losasso C, Belluco S, Cibin V, et al. Antibacterial activity of silver nanoparticles: sensitivity of different Salmonella serovars. *Front Microbiol*. 2014;5:227. doi:10.3389/fmicb.2014.00227
66. Nadtochenko VA, Rincon AG, Stanca SE, Kiwi J. Dynamics of E. coli membrane cell peroxidation during TiO2 photocatalysis studied by ATR-FTIR spectroscopy and AFM microscopy. *J Photochem Photobiol A*. 2005;169(2):131–137.
67. Naumann DSC, Sabisch A, Kastowsky M, Labischinski H. New insights into the phase behaviour of a complex anionic amphiphile: architecture and dynamics of bacterial deep rough lipopolysaccharide membranes as seen by FTIR, X-ray, and molecular modelling techniques. *J Mol Struct*. 1989;214:213–246. doi:10.1016/0022-2860(89)80015-8

68. Mu X, Wang JY, Bai X, et al. Black phosphorus quantum dot induced oxidative stress and toxicity in living cells and mice. *ACS Appl Mater Interfaces*. 2017;9(24):20399–20409. doi:10.1021/acsami.7b02900
69. Banner DJ, Firlar E, Jakubonis J, et al. Correlative ex situ and Liquid-Cell TEM Observation of Bacterial Cell Membrane Damage Induced by Rough Surface Topology. *International Journal of Nanomedicine*. 2020;15:1929.
70. He K, Shokuhfar T, Shahbazian-Yassar R. Imaging of soft materials using in situ liquid-cell transmission electron microscopy. Journal of Physics Condensed Matter: an Institute of Physics journal. 2019;31(10):103001–103001.
71. Ghodsi SM, Megaridis CM, Shahbazian-Yassar R, Shokuhfar T. Advances in Graphene-Based Liquid Cell Electron Microscopy: Working Principles, Opportunities, and Challenges. *Small Methods*. 2019;3(5):1900026.